Eur. Phys. J. B **34**, 25–31 (2003)
DOI: 10.1140/epjb/e2003-00192-5

THE EUROPEAN PHYSICAL JOURNAL B

An ellipsometric investigation of Ag/SiO_2 nanocomposite thin films

R.K. Roy[1], S.K. Mandal[2], D. Bhattacharyya[3], and A.K. Pal[1,a]

[1] Department of Materials Science, Indian Association for the Cultivation of Science, Calcutta 700 032, India
[2] Inter University Consortium for DAE Facilities, Sector III, Block LB/8, Bidhan Nagar, Calcutta 700 098, India
[3] Spectroscopy Division, Bhabha Atomic Research Centre, Mumbai 400 085, India

Received 6 December 2002 / Received in final form 3 April 2003
Published online 23 July 2003 – © EDP Sciences, Società Italiana di Fisica, Springer-Verlag 2003

Abstract. Dielectric properties of silver/SiO_2 nanocomposite thin films grown by high-pressure d.c. sputtering technique were studied by spectroscopic ellipsometry (300–800 nm). The dielectric behavior of the nanocomposite thin films largely depended on the particle size, its number density and the surrounding environments. The films showed semiconductor-like behavior up to a critical particle size and concentration, beyond which the films exhibited the typical surface plasmon resonance characteristics in their optical properties. The refractive index was also found to have a strong dependence on the particle size and its dispersion in the matrix. The results were found to be consistent with those obtained from UV-VIS optical absorbance data. Bruggeman effective medium theory was used to explain the experimental results.

PACS. 78.67.-n Optical properties of nanoscale materials and structures – 78.67.Bf Nanocrystals and nanoparticles

1 Introduction

Noble metal nanoparticles embedded in an insulating host matrix have been extensively studied in recent years due to their novel optical properties which are conducive to various technological applications [1–6]. Their novel optical properties stem from the 3-D quantum confinement of electrons and holes in small volumes. Bulk noble metals exhibit both the free electron and interband transition ($4d \rightarrow 5sp$ for Ag, $5d \rightarrow 6sp$ for Au) behavior depending on the wavelength range. In contrast, noble metal nanoclusters show significant deviation from the free electron behavior and exhibit surface plasmon resonance (SPR) in the optical absorbance spectra due to the collective resonant interaction with electric field. Typical optical features of these nanocomposites are generally studied by optical transmission/absorption [5,7–9], reflection [10,11] and Raman spectroscopy [12–14] and spectroscopic ellipsometry [15,16]. Compared to the other techniques, ellipsometry is a most advantageous tool since it can directly evaluate the dielectric function of the films at a given energy. This dielectric function $\varepsilon(\omega) = \varepsilon_1(\omega)+\mathrm{i}\varepsilon_2(\omega)$ can then be related to the electronic, structural, vibrational and morphological features of the materials [17–20]. For the nanocomposite noble metal films, the energy and width of the plasmon resonance maximum is determined by the real, $\varepsilon_1(\omega)$, and imaginary part, $\varepsilon_2(\omega)$, of the dielectric function respectively. The surface plasmon resonance characteristics are influenced by several physical parameters *e.g.* particle size, metal fraction in the host matrix, nature of the surrounding environment etc. In this communication, we have presented the effect of particle size and volume fraction of the silver nanoparticles embedded in SiO_2 matrix on the dielectric and optical properties obtained through spectroscopic ellipsometric analyses.

2 Experimental

The films were synthesized by using a multi-target high pressure sequential d.c. sputtering apparatus. Both the silver and SiO_2 targets (99.995%) were sputtered intermittently in argon plasma at a system pressure of ~60 Pa and the films were deposited on fused silica substrates. Substrate temperature and deposition time could be varied to obtain films with different particle size ($2R$) and inter-particle spacings as well as the desired thickness. In the present study, three sets of nanocomposite films were deposited as layered structures of SiO_2-substrate/SiO_2/Ag/SiO_2 at substrate temperature 253 K with volume fraction of silver (f) ~0.04, 0.12 and 0.22 respectively. The deposition time for the nanocrystalline Ag layer was varied within 15–120 s in order to obtain films with desired volume fractions. The deposition time for the individual SiO_2 layer was kept the same, 240 s in all the films obtained. The total thickness of the whole structure

[a] e-mail: msakp@iacs.res.in

of $SiO_2/Ag/SiO_2$ layers was varied within 5–30 nm. All the depositions were carried out at ∼1.5 kV and 100 mA with the target (of diameter ∼2.5 cm) and substrate distance of ∼2.5 cm. The details of the deposition system have been described in our earlier reports [21,22].

The ellipsometric data for the films were recorded with a Spectroscopic Phase Modulated Ellipsometer (Model UVISEL^{TM} 460, ISA JOBIN-YVON SPEX) in the wavelength range of 300–800 nm at an angle of incidence of 70°. Microstructural characterization was done by a Hitachi H-600 transmission electron microscope (TEM).

3 Results and discussion

The macroscopic properties of the nanocomposite thin film are determined by the geometry of the individual particles in the matrix. This geometry refers to the size, shape, inter-particle spacings, surface/interface of the nanocrystals and nature of the surrounding environment which solely depends on the growth conditions of the nanocrystals and is influenced by various parameters of synthesis. It is well known that a film containing a dilute dispersion of small spherical metal particles with negligible inter-particle interaction effect [23] would exhibit surface plasmon band in the optical absorption spectra (Mie resonance) due to the interaction with the electric field. With increasing particle concentration, the geometry gets modified with an evolution of increasing particle size, and shape. This could lead to multi-pole interactions among the particles and would increase electron-surface scattering effects [5,24–26]. It would induce either a shift of the Mie resonance band to longer wavelength or a splitting of the dipolar resonance band into two bands, corresponding to the transverse and longitudinal mode of oscillations of the electrons which in turn would depend on the aspect ratio of the nanocrystals. The width of the plasmon band is also strongly dependent on the size and its distribution. It is necessary to mention here that, apart from the particle size and shape, the band position and its width are critically dependent on the type of embedding dielectric matrix [27,28]. The change in electron density at the particle-surface/dielectric interface will have a profound effect on the dielectric behavior. This clearly indicates that any fluctuation in the local dielectric environment of the individual nanocrystals would have a strong effect on the surface plasmon band and the interpretation would be quite complex. So the direct determination of the dielectric function and in turn, interpretation of the optical properties of the nanocomposite films would be much more reliable and straightforward. In this context, spectroscopic ellipsometry can be of very useful as it can directly calculate the dielectric function and is very sensitive to the film growth, compositional fluctuations, sample thickness, surface roughness etc.

The experimental results are discussed with reference to three representative nanocomposite silver films (S-1, S-2 and S-3) with an increasing amount of discrete particle (metal) concentration but without any significant agglomeration. The volume fractions of silver (f) obtained

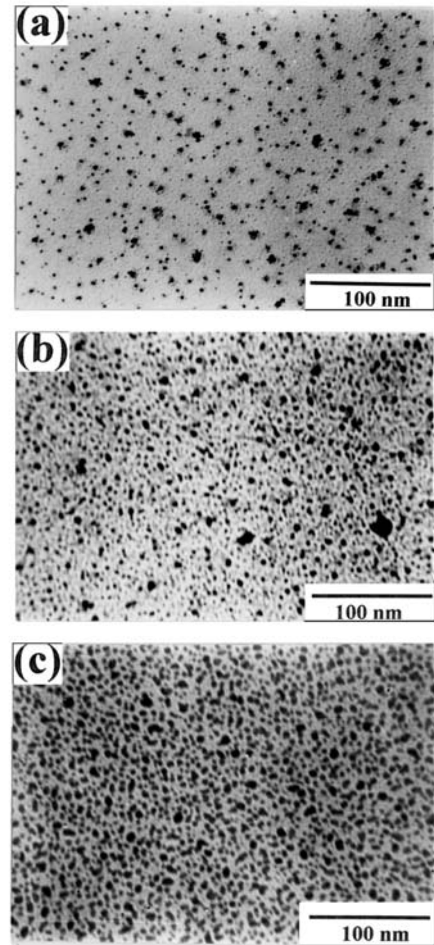

Fig. 1. TEM micrographs of three representative Ag/SiO_2 films deposited at $T_s \sim 253$ K with different volume fraction (f) of silver nanocrystallites: (a) S-1 ($f \sim 0.04$); (b) S-2 ($f \sim 0.12$) and (c) S-3 ($f \sim 0.22$).

from ellipsometry were 0.04, 0.12 and 0.22 for samples S-1, S-2 and S-3 respectively. The average particle size as obtained from TEM (Fig. 1), varied from 1–3 nm as the volume fraction of silver increased from 0.04 to 0.22. The TEM images further showed that the films contained silver nanoparticles with a narrow distribution in size and presumably spherical in shape.

It is necessary to mention here that the optical properties of semicontinuous metal films show anomalous behaviors in the near-infra-red (NIR) and long wavelength regions in the limit of the percolation threshold [10]. With the increase in metal concentration in the insulating matrix, the growth may evolve with irregular shaped percolating clusters providing continuous conducting paths in the film. Near the percolation threshold, application of MG or Bruggeman effective medium theory in describing the optical properties becomes inherently inconsistent with the experimental results and a scaling theory as modeled by Yagil *et al.* [10] was found to give a reasonable description. The effective dielectric constant would lose its significance near the percolation limit. In the composite

films under study, the loading of silver nanocrystallites in the SiO_2 matrix is far below the threshold limit of percolation as is evident from the presence of discrete and isolated Ag nanoparticles (Figs. 1a–c). The film with highest Ag fraction ∼0.22 (Fig. 1c) may be very near to the border line for a percolating network and as such the effect is not pronounced to indicate any anomaly in the plasmon resonance spectra of the composite film. However, further increase in Ag concentration (>0.22 in our case) would lead to evolution of the percolating network and the observed optical properties then should be described by considering the additional surface relaxation for the conduction electrons and a change in the plasma frequency.

In ellipsometry, the variation of the amplitude and the phase difference between the perpendicular (p) and the parallel (s) components of the reflected light polarized with respect to the plane of incidence are measured. In general, reflection causes a change in the relative phase of p and s waves and in the ratio of their amplitudes. The effect of reflection is measured by the two quantities, *viz.* ψ (which measures the amplitude ratio) and $\varDelta$ (which measures the relative phase change). These are given by:

$$\rho = r_p/r_s = \tan\psi \exp(\mathrm{i}\varDelta) \quad (1)$$

where r_p and r_s are the reflection coefficients for the p and s component of the waves respectively. In the Phase Modulated Ellipsometry technique used here [29–32], the reflected light is modulated by a photo-elastic modulator. The modulator is actually a fused silica bar, which is subjected to periodical stress induced by a piezoelectric transducer. The stress creates an optical anisotropy in the silica bar. As a result, the refractive index corresponding to a light beam with its polarization parallel to the strain, differs from the index corresponding to a beam with its polarization perpendicular to the strain. Thus a photoelastic modulator induces a phase shift $\delta(t)$ between the two eigenmodes and the modulated signal takes the general form:

$$I(\lambda, t) = [I_o + I_s \sin\delta(t) + I_c \cos\delta(t)] \quad (2)$$

where,

$$\delta(t) = A_o \sin\omega t \quad (3)$$

where, A_o is the modulation amplitude which is proportional to $(V_m/\lambda), V_m$ being the excitation voltage and λ is the wavelength of light and ω is the modulation frequency (50 kHz in our case).

$$\begin{aligned} I_o = {} & 1 - \cos 2\psi \cos 2A \\ & + \cos 2(P - M) \cos 2M (\cos 2A - \cos 2\psi) \\ & + \sin 2A \cos\varDelta \cos 2(P - M) \sin 2\psi \sin 2M \quad (4) \end{aligned}$$

$$I_s = \sin 2(P - M) \sin 2A \sin 2\psi \sin\varDelta \quad (5)$$

$$\begin{aligned} I_c = {} & \sin 2(P - M)[\sin 2M(\cos 2\psi - \cos 2A) \\ & + \sin 2A \cos 2M \sin 2\psi \cos\varDelta] \quad (6) \end{aligned}$$

where, the angles A, P and M are the respective orientations of the Analyzer, Polarizer and Modulator w.r.t the plane of incidence.

In the present set of measurements, $M = 0°$, $P = 45°$ and $A = 45°$, so that,

$$I_o = 1 \quad (7)$$

$$I_s = \sin 2\psi \sin\varDelta \quad (8)$$

$$I_c = \sin 2\psi \cos\varDelta. \quad (9)$$

The detected signal was processed by a p.c. to determine the parameters I_s and I_c, which in turn generate the parameters of interest *viz.*, ψ and $\varDelta$.

The measured ellipsometry spectra are then fitted with theoretically generated spectra assuming a realistic sample structure. The present samples were deposited by sequential sputtering technique using a multi-target jig so that SiO_2/Ag/SiO_2 structure in nanocrystalline form could be deposited on the substrate. Thus, basically a three layered sample structure: substrate/SiO_2/(Ag+SiO_2)/SiO_2/air would be the most realistic assumption for the theoretical fit. It may be noted here that composite films deposited by co-sputtering would culminate in more complicated assumptions for the structure. The optical constants of the SiO_2 have been supplied from the literature and for Ag nanocrystals also we have used the optical constants of bulk Ag [16,33,34]. In case of composite layers, consisting of Ag and SiO_2, the calculation for the effective optical constants has been done using the Bruggeman Effective Medium Approximation (BEMA) model [35], which describes a composite of aggregated phases or a random mixture microstructure. In the BEMA model the effective medium acts as the host following the expression:

$$f_m \frac{\varepsilon_m - \varepsilon_{\mathit{eff}}}{\varepsilon_m + 2\varepsilon_{\mathit{eff}}} + f_d \frac{\varepsilon_d - \varepsilon_{\mathit{eff}}}{\varepsilon_d - 2\varepsilon_{\mathit{eff}}} = 0 \quad (10)$$

where $\varepsilon_{\mathit{eff}}$, ε_m and ε_d are the dielectric functions of the effective medium, the metal and the dielectric and f_m and f_d are the volume fraction of the metal and the dielectric respectively.

Assuming the above sample structure and using the BEMA model, the theoretical r_p and r_s values and hence ψ and $\varDelta$ spectra are then generated using the standard Fresnel's relations for thin film structures. The measured ellipsometric spectra are then fitted by minimizing the squared difference (χ^2) between the measured and calculated values of the ellipsometric parameters (I_s and I_c) given by:

$$\chi^2 = [1/(2N - P)] \sum_i^N \left[\left(I_{s_i}^{\exp} - I_{s_i}^{\mathrm{cal}}\right)^2 + \left(I_{c_i}^{\exp} - I_{c_i}^{\mathrm{cal}}\right)^2 \right] \quad (11)$$

where, N is the number of data points and P is the number of model parameters. The maximum number of iterations allowed is 100 and the criteria for convergence used is $\delta\chi^2 = 0.000001$. Thickness of the different sublayers and the volume fraction of the different components have been used as the fitting parameters in the above process.

Figures 2a–c show the experimental $\varPsi$ and $\varDelta$ for the films S-1, S-2 and S-3 respectively along with the best

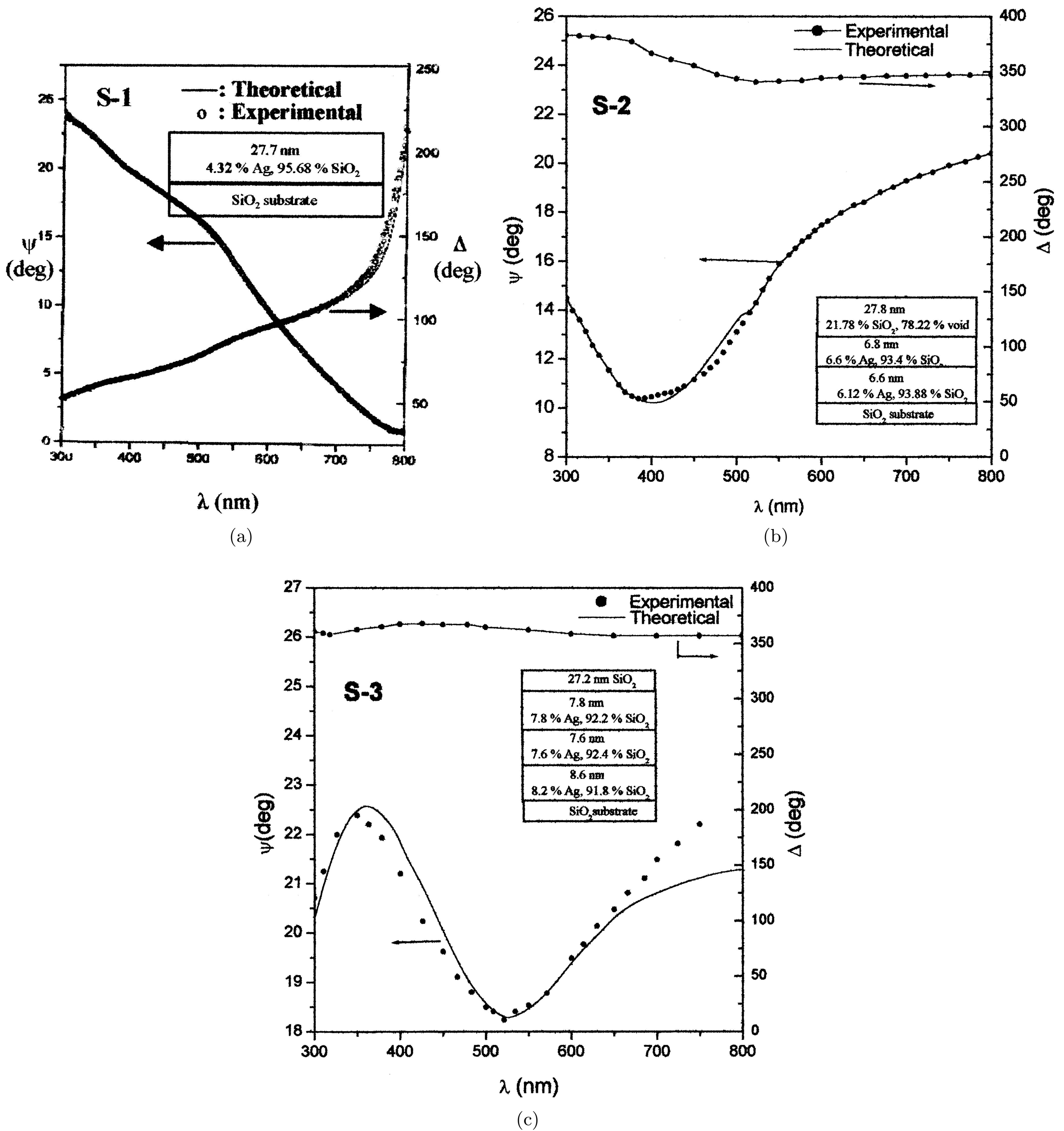

Fig. 2. Variation of Ψ and Δ with the wavelength (λ) of the incident radiation for three representative films with different volume fraction of silver nanoparticles: (a) S-1 ($f \sim 0.04$); (b) S-2 ($f \sim 0.12$) and (c) S-3 ($f \sim 0.22$).

fit theoretical curves over the wavelength range of 300–800 nm. The sample structure obtained for the films from the best fit are also shown in the respective figures. Using the thickness of the samples obtained from the best fit ellipsometric analysis the ψ and Δ spectra are then inverted to get the variation of refractive index (n) and extinction coefficient (k) of the films which are shown in Figures 3a and 3b respectively.

It is evident from the Figures 2a–c that the variation of the relative phase and amplitude of the reflected light with wavelength have a pronounced effect on the silver content of the nanocomposite films. Sample S-1, containing 4% of silver nanoparticles, showed (Fig. 2a) a continuous variation in Ψ and Δ with wavelength (λ). The relative phase change (Ψ) decreased monotonically with increasing wavelength while the relative amplitude change

(Δ) decreased exponentially with the decrease in wavelength. But with the increase in the amount of the volume fraction of silver in the films, variation of both Ψ and Δ with wavelength deviated significantly (Figs. 2b, c) from that obtained for films with lower silver nanoparticle content. The relative amplitude change (Δ) did not show such exponential decrease with decreasing wavelength but rather showed small variation with wavelength. With the increase in silver loading, the relative phase change (Ψ) value for the film (S-2) decreased with decreasing wavelength reaching a minimum around 390 nm. With further increase in Ag content in the film, the relative phase change (Ψ) showed a maximum before it decreased with increasing wavelength. The position of the minimum was found to shift to higher wavelength (~520 nm) for the film S-3 having highest silver content. The results could be explained well if we look at the variation in refractive index (n) and extinction coefficient (k) with λ as obtained from Ψ and Δ values.

Figures 3a and 3b show the obtained values of n and k for the samples S-1, S-2 and S-3 respectively. The extinction coefficients indicated a maximum value at 480 nm and 540 nm for the films S-2 and S-3 respectively. The extinction maximum could be ascribed to the surface plasmon band observed in these films. The broad (FWHM>200 nm) bands are red-shifted with the increase in size and volume fraction of silver. The broadening could be ascribed to very small size of the particles and its distribution. In contrast, for the film S-1, the extinction spectrum did not show any surface plasmon resonance, instead it showed a sharp absorption behavior corresponding to a semiconductor with direct band gap. Similar behavior was observed (Fig. 2a) in the variation of Ψ and Δ with wavelength (λ). This absence of a plasmon resonance peak may be associated with the very small size and very low number density of the silver nanoparticles dispersed in silica matrix. This low-volume-fraction of very small nanocrystallites would render the interactions between the isolated nanoparticles in an external electrical field quite negligible. Thus, the disappearance of the plasmon band and appearance of sharp absorption edge (~ at 350 nm) clearly indicates that there is a critical limit of the particle size and its dispersion within the matrix, below which the surface plasmon band is suppressed and largely broadened. As a consequence, resonant oscillation of the conduction electrons in interaction with the electric field would be replaced by single electron transitions between the discrete energy levels of the silver nanocrystallites [28] and would exhibit semiconductor like optical absorption. Near the surface plasmon band, n values also showed an anomalous dispersion and this is consistent with the Kramers-Kronig relation [5]. Also, the increase in n is abrupt (Fig. 3a) near the absorption edge for the sample S-1 and exceeds the bulk value of n of both Ag and SiO_2.

The results obtained from spectro-ellipsometric investigations can also be compared with that obtained from optical absorbance measurements. Figure 4 shows the plot of extinction coefficient (k) with wavelength for the samples S-1, S-2 and S-3. The surface plasmon bands appeared for sample S-2 and S-3 at 475 nm and 539 nm respectively. The band positions agreed well with the ellipsometric measurements but there is a slight disagreement on the width and shape of the resonance band. It also showed the sharp semiconductor like absorption edge for the sample S-1 as obtained from ellipsometric data. It is to be mentioned here that the line-shape of the surface plasmon bands are asymmetric and linewidths are

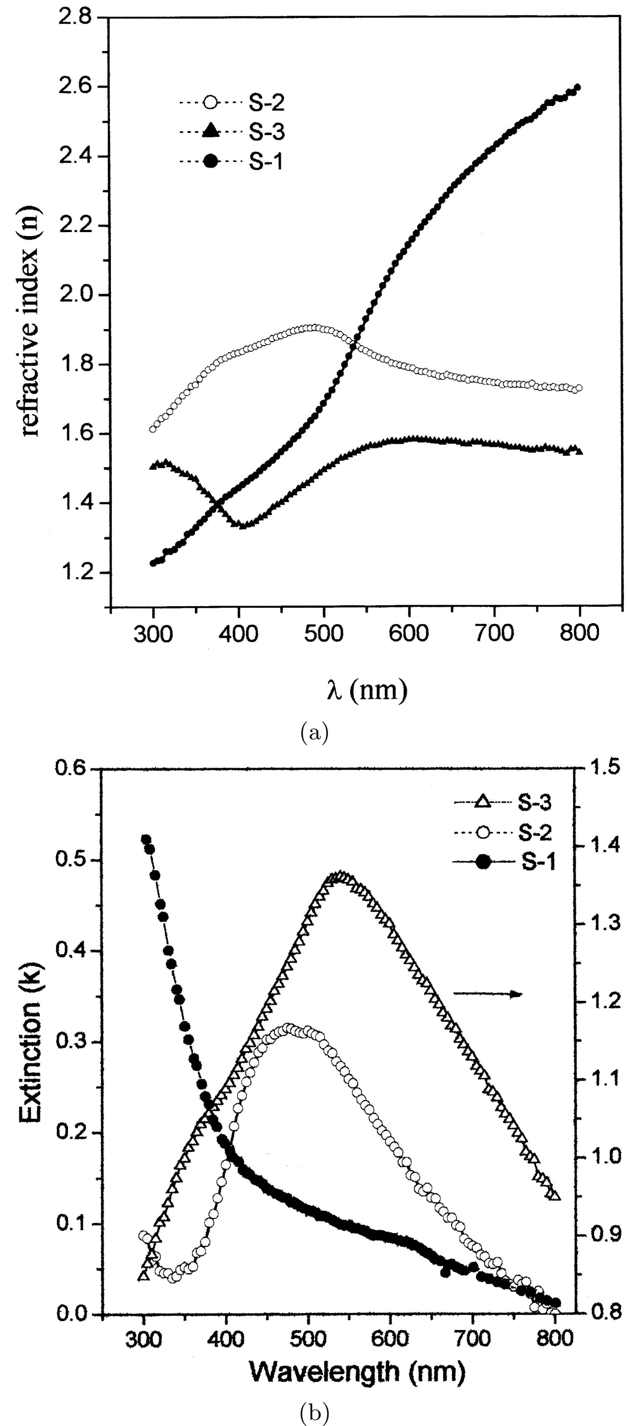

Fig. 3. Variation of: (a) refractive index, n and (b) extinction coefficient, k with λ for three representative films.

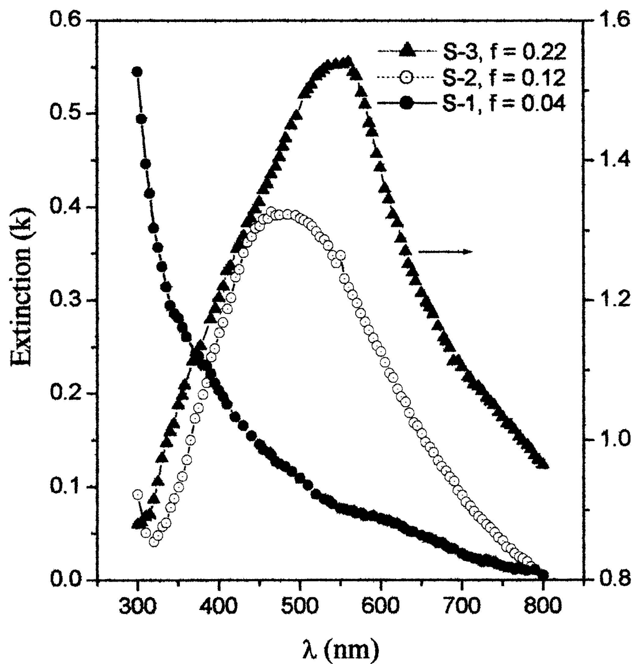

Fig. 4. Variation of extinction coefficient (k) with wavelength (λ) obtained from optical absorbance measurements for three representative films with different silver loadings.

quite large (FWHM>200 nm). The SPR lineshape and its width are found to have a strong dependence on the size of the nanoparticles, their shape and distribution, and the embedding matrix [36]. The size ($2R$) dependence linewidth (Γ) of the SPR as modeled by Kawabata and Kubo [37] is expressed as,

$$\Gamma = \Gamma_i + \Delta\Gamma(R) \tag{12}$$

where Γ_i is the intrinsic linewidth arising from the bulk properties and $\Delta\Gamma(R)$ is the size dependent ($\propto 1/R$) contribution to the total linewidth of the SPR. The distribution of the particles may also cause an inhomogeneous broadening of resonance band. In our case, the observed large linewidth could not simply be attributed to the dependence on size and its distribution. In fact, for small clusters <5 nm embedded in a matrix, as in our case, apart from size-dependent contributions, the additional effect probably stems from Ag nanoparticles/SiO_2 interface properties and is ignored in equation (12). Hövel *et al.* [38] demonstrated that under the excitation of light, the excited electrons upon colliding with the interface are transferred to the affinity levels of the surrounding matrix and back again. The surrounding matrix acts as an efficient heat bath to dissipate the energy and momentum of the transferred electrons and causes substantial inelastic scattering of the electrons at the interface. The collective excitation of the resonant absorption band gets disturbed by the relaxation of the electrons in the excited states of the surrounding SiO_2 matrix and profoundly affects the energy and width of the resonance state. In fact, besides size-dependence, the collective contribution of the decay of the excited electrons, electron-hole pairs, electro-phonon interactions, and scattering at structural defects in the bulk and at surface could be the possible sources for the observed experimental broadening of the SPR in our Ag/SiO_2 nanocomposite films [39].

The ellipsometric results are found to be very sensitive to the assumed values of physical parameters of the individual layers in the fitting procedure. In any ellipsometric fitting process, it is customary to try the fitting using the single layer model first and then complexity of the sample structure is increased from single layer to bi-layer to tri-layer models to get the best fits. It may be stressed here that the composite layers in nanocrystalline form were deposited by sequential sputtering technique using a multi-target sputtering jig. Here, ascribing a three layered structure to the composite films deposited would be a realistic assumption. The middle layers constituting different loading of silver nanoparticles arise due to slight fluctuation in the sputtering rate and corresponding inter-mixing of silver and SiO_2 nanoparticles at the interfaces. This effect became more pronounced as silver loading was increased and it was observed that in case of higher loading (for Sample-3) of silver (having substantially higher sputtering yield) it becomes increasing difficult to keep the SiO_2 layer thickness constant for all the depositions. Increase in SiO_2 layer thickness becomes necessary to impart the desired silver loading. Thus, for films with higher silver loading, one may expect (as observed in Sample-3) the contribution from an additional SiO_2 layer at the top. It may be worthwhile to note that in the case of metal composite films grown by co-sputtering technique where the film is regarded as a heterogeneous mixture of metals and voids, consideration of the number of layers constituting the structure for generating the theoretical fit would have been more complicated. The void fraction is found to decrease with the increase in thickness of the films [40]. Bruggeman effective medium theory is found to provide a more realistic approach than other models such as Maxwell-Garnett (MG) or Lorentz-Lorentz (LL) [41,42] since it treats all the constituents of the medium, as well as voids, on equal basis.

4 Conclusion

To summarize, we have studied the optical properties from the data obtained from spectroscopic ellipsometry for silver nanocomposite thin films. Nanocomposite Ag/SiO_2 films were prepared by a high-pressure sequential sputtering technique with different particle sizes and number densities of the silver nanoparticles. The metal particle densities could be varied in the matrix by varying the relative time of sputtering of the two targets. The sputtering rate and the substrate temperature were appropriately adjusted to obtain a very small size of particles (1–3 nm) without any significant agglomerations up to a certain thickness. The films showed the surface plasmon resonance behavior up to a critical size (<4 nm) and concentration of the nanoparticles ($f < 0.05$), below which the film exhibited semiconductor-like behavior due to the single electron transitions between the quantized energy levels of silver

nanocrystallites. The extinction coefficients (k) obtained from ellipsometry and optical absorption measurements are found to be consistent with each other. The refractive index (n) was also found to show an abrupt change around the plasmon band and was found to exceed the bulk values. Bruggeman effective medium theory was applied to theoretically simulate the experimental results.

One of us, R.K.R. wishes to thank the Council of Scientific and Industrial Research, Government of India, for granting him a fellowship for executing this work.

References

1. H.E. Katz, Science **254**, 1485 (1991)
2. Y. Hamanaka, A. Nakamura, S. Omi, N. Del Fatti, F. Vallee, C. Flytzanis, Appl. Phys. Lett. **75**, 1712 (1999)
3. K. Matsubara, S. Kawata, N. Minami, Appl. Opt. **27**, 1160 (1988)
4. J.S. Schildkraut, Appl. Opt. **27**, 4587 (1988)
5. U. Kreibig, M. Vollmer, *Optical Properties of Metal Clusters* (Springer, 1995)
6. M. Sugiyama, S. Inasawa, S. Koda, T. Hirose, T. Yonekawa, T. Omatsu, Appl. Phys. Lett. **79**, 1528 (2001)
7. J.B. Jackson, N.J. Halas, J. Phys. Chem. B **105**, 2743 (2001)
8. R.H. Doremus, J. Appl. Phys. **37**, 2775 (1966)
9. C.G. Granqvist, O. Hunderi, Phys. Rev. B **16**, 3513 (1977)
10. Y. Yagil, P. Gadenne, C. Julien, G. Deutscher, Phys. Rev. B **46**, 2503 (1992)
11. L.C. Nistor, J. van Landuyt, J.D. Barton, D.E. Hole, N.D. Skelland, P.D. Townsend, J. Non-Cryst. Sol. **162**, 217 (1993)
12. D.A. Weitz, T.J. Gramila, A.Z. Genack, J.I. Gersten, Phys. Rev. Lett. **45**, 355 (1980)
13. G. Mariotto, M. Montanga, G. Viliani, E. Duval, S. Lefrant, E. Rzepka, C. Mai, Europhys. Lett. **6**, 239 (1988)
14. M. Fujii, Phys. Rev. B **44**, 6243 (1991)
15. D. Dalacu, L. Martinu, J. Appl. Phys. **87**, 228 (2000)
16. J.C.G. de Sande, R. Serna, J. Gonzalo, C.N. Afonso, D.E. Hole, A. Naudon, J. Appl. Phys. **91**, 1536 (2002)
17. *Spectroscopic Ellipsometry*, edited by A.C. Boccara, C. Pickering, J. Rivory (Elsevier, Amsterdam, 1993)
18. S. Logothetidis, J. Petalas, M. Cardona, T.D. Monstakas, Phys. Rev. B **50**, 18017 (1994)
19. D.E. Aspnes, W.E. Quinn, S. Gregory, Appl. Phys. Lett. **57**, 2707 (1990)
20. S. Logothetidis, J. Petalas, J. Appl. Phys. **80**, 1768 (1996)
21. S.K. Mandal, S. Chaudhuri, A.K. Pal, Thin Solid Films, **350**, 209 (1999)
22. S.K. Mandal, A. Ganguly, S. Chaudhuri, A.K. Pal, Vacuum **52**, 485 (1999)
23. G. Mie, Ann. Phys. (Leipzig) **25**, 377 (1908)
24. H. Ehrenreich, H.R. Philipp, Phys. Rev. B **128**, 1662 (1962)
25. Z. Liu, H. Wang, H. Li, X. Wang, Appl. Phys. Lett. **72**, 1823 (1998)
26. S. Link, M.A. El-Sayed, J. Phys. Chem. B **103**, 4212 (1999)
27. K.P. Charle, L. Konig, S. Nepijko, I. Rabin, W. Schulze, Cryst. Res. Technol. **33**, 1085 2 0 (1998)
28. L. Yang, G.H. Li, L.D. Zhang, Appl. Phys. Lett. **76**, 1537 (2000)
29. D. Bhattacharyya, N.K. Sahoo, S. Thakur, N.C. Das, Thin Solid Films **360**, 96 (2000)
30. D. Bhattacharyya, N.K. Sahoo, S. Thakur, N.C. Das, Appl. Optics **40**, 1707 (2001)
31. G.K. Mor, L.K. Malhotra, D. Bhattacharyya, J. Appl. Phys. **90**, 1795 (2001)
32. D. Bhattacharyya, N.K. Sahoo, S. Thakur, N.C. Das, Thin Solid Films **416**, 97 (2002)
33. E.D. Palik, *Handbook of Optical Constants of Solids* (Academic Press, New York, 1985)
34. D.E. Gray, *American Institute of Physics Handbook* (McGraw-Hill, New York, 1972)
35. D.A.G. Bruggeman, Ann. Phys. **24**, 638 (1935)
36. U. Kreibig, L. Genzel, Surf. Sci. **156**, 678 (1985)
37. A. Kawabata, R. Kubo, J. Phys. Soc. Jpn **21**, 1765 (1966)
38. H. Hövel, S. Fritz, A. Hilger, U. Kreibig, M. Vollmer, Phys. Rev. B **48**, 18 178 (1993)
39. A. Goldman, R. Atzdorf, F. Theilman, Surf. Sci. **414**, L932 (1998)
40. S. Kundu, S. Hazra, S. Banerjee, M.K. Sanyal, S.K. Mandal, S. Chaudhuri, A.K. Pal, J. Phys. D **31**, L73 (1998)
41. J.C. Maxwell-Garnett, Phil. Trans. R. Soc. **203**, 385 (1904)
42. C.G. Granqvist, O. Hunderi, Phys. Rev. B **16**, 3513 (1977)